Inorg. Chem. **2005**, *44*, 638–648

Dramatic Variation of Magnetic Exchange through Double End-on Azide Bridges in a Series of Ladder-Like Copper(II) Coordination Polymers

Jonathan D. Woodward,[†] Rénal V. Backov,[†] Khalil A. Abboud,[†] D. Dai,[‡] H.-J. Koo,[‡] M.-H. Whangbo,*[,‡] Mark W. Meisel,*[,§] and Daniel R. Talham*[,†]

Departments of Chemistry and Physics and Center for Condensed Matter Sciences, University of Florida, Gainesville, Florida 32611, and Department of Chemistry, North Carolina State University, Raleigh, North Carolina 27695-8204

Received June 24, 2004

Three ladder-like coordination polymers, $[Cu_2(phprpy)_2\text{-}\mu\text{-}(N_3)_2(N_3)_2]$, **1**; $[Cu_2(terpy)_2\text{-}\mu\text{-}(N_3)_4Cu_2\text{-}\mu\text{-}(N_3)_2(N_3)_2]$, **2**; and $[Cu_2(terpy)_2\text{-}\mu\text{-}(N_3)_2(N_3)_2Cu_3\text{-}\mu\text{-}(N_3)_4(N_3)_2]$, **3**, consisting of Cu^{2+} ions with double end-on azide bridges were synthesized, their crystal structures and magnetic properties were determined, and spin dimer analysis was performed to explain the signs and strengths of their strong spin exchange interactions [phprpy is 4-(3-phenylpropyl)pyridine and terpy is 2,2′:6,2″-terpyridine]. Although these compounds have ladder-like arrangements of Cu^{2+} ions, their magnetic structures are described as isolated dimers for **1** and **2** and as isolated trimers for **3**. The predominant spin exchange paths in **1**–**3** have double end-on azide bridges linking adjacent Cu^{2+} ions, and the geometrical parameters of these bridging structures are similar. However, the spin dimer of **1** exhibits a strong ferromagnetic coupling; that of **2**, a strong antiferromagnetic coupling; and that of **3**, a weak ferromagnetic coupling. These findings are well explained by the present spin dimer analysis and show that the nature and geometry of the nonbridging ligands can have a strong influence on the sign and strength of the spin exchange interaction between Cu^{2+} ions connected by double end-on azide bridges.

Introduction

The azide anion, N_3^-, is one of the more commonly employed pseudohalide bridging ligands in the design of polynuclear transition metal complexes and coordination solids with characteristic and tunable physical properties.[1,2] In general, two types of bridging modes are frequently observed for the azido ligand in transition metal complexes, the μ-(1,1) or "end-on" mode and the μ-(1,3) or "end-to-end" mode.[1,3−7] These modes are also seen as double bridges, as illustrated in Figure 1. The azide anion often mediates superexchange interactions between adjacent magnetic transition metal cations, and a diverse array of magnetic properties arise from variable bridging modes and bonding arrangements.[1] Several attempts have been made to correlate

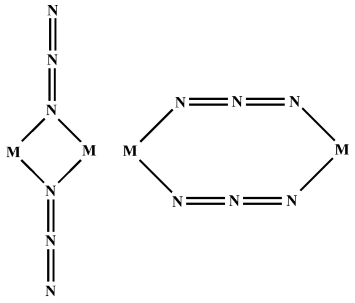

a **b**

Figure 1. Azide bridging modes: (a) double end-on and (b) double end-to-end.

* To whom correspondence should be addressed. E-mail: talham@chem.ufl.edu (D.R.T.), meisel@phys.ufl.edu (M.W.M.), Mike_Whangbo@ncsu.edu (M.-H.W.).

[†] Department of Chemistry, University of Florida.

[‡] Department of Physics and Center for Condensed Matter Sciences, University of Florida.

[§] North Carolina State University.

(1) Kahn, O. *Molecular Magnetism*; VCH: New York, 1993.
(2) Miller, J. S.; Drilon, M., Eds. *Magnetism: Molecules to Materials*; Wiley-VCH: Weinheim, Germany, 2002.
(3) Ribas, J.; Escuer, A.; Monfort, M.; Vicente, R.; Cortes, R.; Lezama, L.; Rojo, T. *Coord. Chem. Rev.* **1999**, *193*, 1027.
(4) Abu-Youssef, M. A. M.; Escuer, A.; Gatteschi, D.; Goher, M. A. S.; Mautner, F. A.; Vicente, R. *Inorg. Chem.* **1999**, *38*, 5716.
(5) Bkouche-Waksman, I.; Boillot, M. L.; Khan, O.; Sikorav, S. *Inorg. Chem.* **1984**, *23*, 4454.
(6) Sikorav, S.; Bkouche-Waksman, I.; Kahn, O. *Inorg. Chem.* **1984**, *23*, 490.
(7) Kahn, O.; Sikorav, S.; Gouteron, J.; Jeannin, S.; Jeannin, Y. *Inorg. Chem.* **1983**, *22*, 2877.

10.1021/ic049175q CCC: $30.25
Published on Web 01/13/2005

the magnetic properties of azide-containing clusters and networks with their bridging modes.[6−13] The symmetric double end-on bridge typically mediates strong ferromagnetic exchange interactions between adjacent magnetic ions,[7,14−19] and the symmetric end-to-end bridge, strong antiferromagnetic exchange interactions.[6,20−24] In contrast, asymmetric bridges can mediate either weak ferromagnetic or antiferromagnetic exchange.[25−33] The simultaneous presence of both bridging azide modes leads to more complex magnetic behavior.[4,34,35]

As part of an effort to develop new examples of ladder-like coordination polymers, we prepared three new compounds based on Cu^{2+} ions with azide bridges, $[Cu_2(phprpy)_2$-μ-$(N_3)_2(N_3)_2]$, **1**; $[Cu_2(terpy)_2$-μ-$(N_3)_4Cu_2$-μ-$(N_3)_2(N_3)_2]$, **2**; and $[Cu_2(terpy)_2$-μ-$(N_3)_2(N_3)_2Cu_3$-μ-$(N_3)_4(N_3)_2]$, **3** [phprpy is 4-(3-phenylpropyl)pyridine and terpy is 2,2′:6′,2″-terpyridine]. These compounds have in common double end-on azide bridges that link Cu^{2+} ions into $Cu(N_3)_2Cu$ dimeric cores for **1** and **2** and a $Cu(N_3)_2Cu(N_3)_2Cu$ trimeric core for **3**.

The new compounds exhibit the structural features of a ladder, but their magnetic properties are not those of spin ladders. However, an interesting feature that arises despite similar geometries is that the double end-on azide bridges exhibit very different magnetic exchange interactions in the three compounds, ranging from strongly ferromagnetic in **1** to weakly ferromagnetic in **3** to strongly antiferromagnetic in **2**. It has been pointed out[36,37] that the strong spin exchange paths of a magnetic solid do not necessarily have the same geometrical features as the covalent bonds that link its magnetic ions. To properly interpret the magnetic properties of **1**−**3**, it is helpful to identify their strongly interacting spin units on the basis of appropriate electronic structure considerations. In the present work, we describe the structural and magnetic properties of compounds **1**−**3** and analyze their spin structures on the basis of both crystal structure and spin dimer analysis. The results show how the nature and the geometry of the nonbridging ligands can strongly influence the spin exchange interaction between Cu^{2+} ions connected by the same double end-on azide bridge.

Experimental Section

Synthesis. Copper(II) perchlorate hexahydrate (98%), 2,2′:6′,2″-terpyridine (terpy) (98%), 4-(3-phenylpropyl)pyridine (phprpy) (97%), and sodium azide (99%) were purchased from Aldrich Chemical Co. Dimethyl sulfoxide (99.9%) was purchased from Fisher Scientific. All reagents were used without further purification. All reactions and crystallizations were performed under ambient conditions. Elemental analyses were performed by the University of Florida Spectroscopic Services Laboratory.

Caution! Although no violent decomposition of the title compounds was observed, azido complexes of metal ions are potentially explosive. Only a small amount of materials should be prepared and handled with care.

$[Cu_2(phprpy)_2$-μ-$(N_3)_2(N_3)_2]$, 1. A solution containing 105 mg of phprpy (0.532 mmol) dissolved in 20 mL of DMSO was added, dropwise, to a solution containing 800 mg of $Cu(ClO_4)_2 \cdot 6H_2O$ (2.16 mmol) dissolved in 20 mL of DMSO. A solution containing 344 mg of NaN_3 (5.29 mmol) dissolved in 20 mL of DMSO was then added dropwise, producing a dark green solution. After approximately 1 week, green-black needles of **1** crystallized and were collected and washed with ethanol (yield 61%). Anal. Calcd for $Cu_2C_{28}H_{30}N_{14}$: C, 48.75%; H, 4.39%; N, 28.44%. Found: C, 47.92%; H, 4.29%; N, 28.26%.

$[Cu_2(terpy)_2$-μ-$(N_3)_4Cu_2$-μ-$(N_3)_2(N_3)_2]$, 2. A solution containing 80 mg of terpy (0.343 mmol) dissolved in 10 mL of DMSO was added, dropwise, to a solution containing 800 mg of $Cu(ClO_4)_2 \cdot 6H_2O$ (2.16 mmol) dissolved in 10 mL of DMSO. A solution containing 501 mg of NaN_3 (7.71 mmol) dissolved in 20 mL of DMSO was then added dropwise, to produce a dark green solution. After approximately 1 week, green-black needles of **2** formed and were collected by vacuum filtration and washed with ethanol (yield 64%). Anal. Calcd for $Cu_4C_{30}H_{22}N_{30}$: C, 34.09%; H, 2.10%; N, 39.76%. Found: C, 34.00%; H, 1.99%; N, 39.46%.

(8) Hay, P. J.; Thibeault, J. C.; Hoffmann, R. *J. Am. Chem. Soc.* **1975**, *97*, 4884.
(9) Kahn, O. *Inorg. Chim. Acta* **1982**, *62*, 3.
(10) Willet, R. D.; Gatteschi, D.; Kahn, O. *Magneto-Structural Correlations in Exchanged Coupled Systems*; Reidel Publishing Company: Dordrecht, The Netherlands, 1985.
(11) Tandon, S. S.; Thompson, L. K.; Manuel, M. E.; Bridson, J. N. *Inorg. Chem.* **1994**, *33*, 5555.
(12) Thompson, L. K.; Tandon, S. S. *Inorg. Chem.* **1995**, *34*, 2356.
(13) Kahn, O. *Angew. Chem., Int. Ed. Engl.* **1985**, *24*, 834.
(14) Cortes, R.; Pizarro, J. L.; Lezama, L.; Arriortua, M. I.; Rojo, T. *Inorg. Chem.* **1994**, *33*, 2697.
(15) Ribas, J.; Monfort, M.; Diaz, C.; Bastos, C.; Solans, X. *Inorg. Chem.* **1994**, *34*, 484.
(16) Ruiz, E.; Cano, J.; Alvarez, S.; Alemany, P. *J. Am. Chem. Soc.* **1998**, *120*, 11122.
(17) Vicente, R.; Escuer, A.; Ribas, J.; Fallah, M. S. E.; Solans, X.; Font-Bardia, M. *Inorg. Chem.* **1993**, *32*, 1920.
(18) Ribas, J.; Monfort, M.; Costa, R.; Solans, X. *Inorg. Chem.* **1993**, *32*, 695.
(19) Cortes, R.; Urtiaga, M. K.; Lezama, L.; Larramendi, J. I. R.; Arriortua, M. I.; Rojo, T. *J. Chem. Soc., Dalton Trans.* **1993**, 3685.
(20) Escuer, A.; Vicente, R.; Ribas, J.; Fallah, M. S. E.; Solans, X.; Font-Bardia, M. *Inorg. Chem.* **1993**, *32*, 3727.
(21) deBiani, F. F.; Ruiz, E.; Cano, J.; Novoa, J. J.; Alvarez, S. *Inorg. Chem.* **2000**, *39*, 3221.
(22) Ribas, J.; Monfort, M.; Diaz, C.; Bastos, C.; Solans, X. *Inorg. Chem.* **1993**, *32*, 3557.
(23) Cortes, R.; Urtiaga, M. K.; Lezama, L.; Pizarro, J. L.; Goni, A.; Arriortua, M. I.; Rojo, T. *Inorg. Chem.* **1994**, *33*, 4009.
(24) Pierpont, C. G.; Hendrickson, D. N.; Duggan, D. M.; Wagner, F.; Barefield, E. K. *Inorg. Chem.* **1975**, *14*, 604.
(25) Comarmond, J.; Plumere, P.; Lehn, J. M.; Angus, Y.; Louis, R.; Weiss, R.; Khan, O.; Morgesten-Badarau, I. *J. Am. Chem. Soc.* **1982**, *104*, 6330.
(26) Munno, G. D.; Lombardi, M. G.; Paoli, P.; Lloret, F.; Julve, M. *Inorg. Chim. Acta* **1998**, *282*, 252.
(27) Shen, Z.; Zuo, J. L.; Gao, S.; Song, Y.; Che, C. M.; Fun, H. K.; You, X. Z. *Angew. Chem., Int. Ed.* **2000**, *39*, 3633.
(28) Dalai, S.; Mukherjee, P. S.; Drew, M. G. B.; Lu, T. H.; Chaudhuri, N. R. *Inorg. Chim. Acta* **2002**, *335*, 85.
(29) Mukherjee, P. S.; Maji, T. K.; Mostafa, G.; Mallah, T.; Chaudhuri, N. R. *Inorg. Chem.* **2000**, *39*, 5147.
(30) Mukherjee, P. S.; Dalai, S.; Mostafa, G.; Lu, T. H.; Rentschler, E.; Chaudhuri, N. R. *New J. Chem.* **2001**, *25*, 1203.
(31) Mukherjee, P. S.; Maji, T. K.; Escuer, A.; Vincente, R.; Ribas, J.; Rosair, G.; Mautner, F. A.; Chadhuri, N. R. *Eur. J. Inorg. Chem.* **2002**, 943.
(32) Maji, T. K.; Mukherjee, P. S.; Mostafa, G.; Mallah, T.; Cano-Boquera, J.; Chaudhuri, N. R. *Chem. Commun.* **2001**, 1012.
(33) Hong, C. S.; Koo, J.; Son, S. K.; Lee, Y. S.; Kim, Y. S.; Do, Y. *Chemistry* **2001**, *2001*, 4243.
(34) Abu-Youssef, M. A. M.; Drillon, M.; Escuer, A.; Goher, M. A. S.; Mautner, F. A.; Vicente, R. *Inorg. Chem.* **2000**, *39*, 5022.
(35) Abu-Youssef, M. A. M.; Escuer, A.; Goher, M. A. S.; Mautner, F. A.; Reiss, G.; Vicente, R. *Angew. Chem., Int. Ed. Engl.* **2000**, *39*, 1624.
(36) Whangbo, M.-H.; Koo, H.-J.; Dai, D. *J. Solid State Chem.* **2003**, *176*, 417.
(37) Whangbo, M.-H.; Koo, H.-J.; Dai, D. *Inorg. Chem.* **2003**, *42*, 3898.

Table 1. Summary of Crystallographic Data for Compounds **1**−**3**

	1	**2**	**3**
empirical formula	$CuC_{14}H_{15}N_7$	$Cu_2C_{15}H_{11}N_{15}$	$Cu_{2.5}C_{15}H_{11}N_{18}$
formula weight	689.74	528.47	602.27
space group	monoclinic, *P*2(1)/*n*	monoclinic, *P*2(1)/*n*	triclinic, $P\bar{1}$
a, Å	5.2066(2)	14.4872(8)	6.6035(6)
b, Å	10.7847(4)	7.1430(4)	12.660(1)
c, Å	27.069(1)	18.454(1)	13.110(1)
α, deg	90	90	88.682(2)
β, deg	91.620(1)	95.719(1)	76.278(2)
γ, deg	90	90	82.819(2)
V, Å^3	1519.4(1)	1900.2(2)	1056.4(1)
Z	2	4	2
T, K	173(2)	173(2)	173(2)
λ(Mo Kα), Å	0.71073	0.71073	0.71073
ρ_{calc}, g cm^{-3}	1.508	1.847	1.893
μ, mm^{-1}	1.445	2.280	2.552
R1 (wR2)[a]	0.0318 (0.0699)	0.0386 (0.0969)	0.0439 (0.0837)

[a] $R1 = \sum(||F_o| - |F_c||)/\sum|F_o|$. $wR2 = [\sum[w(F_o^2 - F_c^2)^2]/\sum|[w(F_o^2)^2]]^{1/2}$. $S = [\sum[w(F_o^2 - F_c^2)^2]/(n - p)]^{1/2}$. $w = 1/[\sigma^2(F_o^2) + (0.0370p)^2 + 0.31p]$. $p = [\max(F_o^2,0) + 2F_c^2]/3$.

[Cu_2(terpy)$_2$-*μ*-$(N_3)_2(N_3)_2Cu_3$-*μ*-$(N_3)_4(N_3)_2$], 3. A solution containing 80 mg of terpy (0.343 mmol) dissolved in 10 mL of DMSO was added, dropwise, to a solution containing 800 mg of $Cu(ClO_4)_2 \cdot 6H_2O$ (2.16 mmol) dissolved in 10 mL of DMSO. A solution containing 344 mg of NaN_3 (5.29 mmol) dissolved in 20 mL of DMSO was then added dropwise giving a dark green solution. After approximately 1 week, dark green-black needles of **3** crystallized and were collected and washed with ethanol (yield 58%). Anal. Calcd for $Cu_5C_{30}H_{22}N_{36}$: C, 29.91%; H, 1.84%; N, 41.89%. Found: C, 30.03%; H, 1.71%; N, 41.64%.

X-ray Structure Determination. Dark green needles of **1** (0.45 × 0.12 × 0.04 mm^3), **2** (0.46 × 0.10 × 0.03 mm^3), and **3** (0.17 × 0.07 × 0.02 mm^3) were selected for X-ray diffraction analysis. Each crystal was mounted on a glass fiber under nitrogen gas. The same data collection process was used for each sample. Data were collected at 173 K on a Siemens SMART PLATFORM equipped with a CCD area detector and a graphite monochromator utilizing Mo Kα radiation ($\lambda = 0.71073$ Å). The cell parameters were refined using up to 8192 reflections. A hemisphere of data (1381 frames) was collected using the *ω*-scan method (0.3° frame width). The first 50 frames were remeasured at the end of data collection to monitor instrument and crystal stability (maximum correction of *I* was <1%). Absorption corrections by integration were applied based on measured indexed crystal faces.

All structures were solved by the Direct Methods in SHELXTL6 and refined using full-matrix least squares.[38] The non-H atoms were treated anisotropically, whereas the hydrogen atoms were calculated in ideal positions and were refined by riding on their respective carbon atoms. For **1**, the asymmetric unit consists of a half-dimer. Part of the pyridine moiety and that of the propyl fragment, −C6-(H_2)C7(H_2)−, of phprpy are both disordered, but the N1 atom of phprpy is not. The disorder was refined in terms of two conformations. Their site occupation factors were refined to 0.56(1) for the major conformation and consequently 0.44(1) for the minor conformation. A total of 264 parameters were refined using F^2 in the final cycle using 3477 reflections with $I > 2\sigma(I)$ to yield R1 = 3.18% and wR2 = 6.99%. For **2**, the asymmetric unit consists of a half-tetramer. A total of 289 parameters were refined using F^2 in the final cycle using 4330 reflections with $I > 2\sigma(I)$ to yield R1 = 3.86% and wR2 = 9.69%. For **3**, the asymmetric unit consists of a half-pentamer. A total of 323 parameters were refined using F^2 in the final cycle using 4771 reflections with $I > 2\sigma(I)$ to yield R1 = 4.39% and wR2 = 8.37%.

Magnetic Measurements. Bulk magnetization measurements were carried out using a standard Quantum Design MPMS SQUID magnetometer. The samples consisted of randomly oriented single crystals with a total mass of 40.8 mg for **1**, 96.3 mg for **2**, and 57.7 mg for **3**. A polyethylene canister and plastic straw were used as the sample holder during the measurements. Slight pressure was applied with the canister lid to prevent motion of the sample. Magnetization versus temperature measurements were run from 2 to 300 K. The sample was zero-field-cooled to 2 K before a measuring field of 100 G was applied and the data set was then taken while the sample was warmed from the lowest temperature. Measurements of magnetization versus field were performed at 2 K over the range of 0−50 kG. The background signals arising from the canister and straw were measured independently and subtracted from the results. For each compound the diamagnetic contributions, χ_D, estimated from Pascal's constants, were $\chi_D = -345.52 \times 10^{-6}$ emu mol^{-1} for **1**, $\chi_D = -452.08 \times 10^{-6}$ emu mol^{-1} for **2**, and $\chi_D = -491.10 \times 10^{-6}$ emu mol^{-1} for **3**.[1,39]

Results and Discussion

Compound Synthesis. Compounds **2** and **3** were synthesized from DMSO by the direct combination of $Cu(ClO_4)_2 \cdot 6H_2O$ and terpyridine with NaN_3 under normal laboratory conditions. In contrast, compound **1** was obtained by employing phprpy as the ancillary ligand. All products crystallized as small, dark green needles by slow evaporation of the solvent within 1 week. Extended structures formed only when the organic ligand was present in substoichiometric quantities. When the terpyridine was added in stoichiometric amounts, crystals of a dinuclear compound, $[Cu(terpy)(N_3)]_2(ClO_4)_2$, similar to the previously reported $[Cu(terpy)(N_3)]_2(PF_6)_2$,[40] were obtained. It is interesting to point out that although compound **2** requires more NaN_3 in the synthesis and crystallization, it contains less azide within its structure than compound **3**.

Crystal structures. Crystallographic and structural refinement data for compounds **1**−**3** are listed in Table 1, and selected bond lengths and angles are included in Tables 2−4, respectively. Tables of atomic coordinates and thermal displacement parameters and complete listings of bond angles

(38) Sheldrick, G. M. SHELXTL6, 6th ed.; Bruker-AXS: Madison, WI, 2000.
(39) Carlin, R. L. *Magnetochemistry*, 1st ed.; Springer-Verlag: Berlin, 1986.
(40) Arriortua, M. I.; Urtiaga, M. K.; Insausti, M.; Mesa, J. L.; Rojo, T. *Polyhedron* **1991**, *10*, 2451.

Table 2. Selected Bond Lengths (Å) and Angles (deg) for Compound **1**

Cu−N5	1.9568(18)	Cu−N2A	1.9934(16)
Cu−N1	1.9747(17)	Cu−N2	1.9968(15)
N5−Cu−N1	96.60(7)	N2a−Cu−N2	78.08(7)
N5−Cu−N2A	164.38(8)	N3−N2−CuA	126.92(13)
N1−Cu−N2A	94.20(7)	N3−N2−Cu	124.37(14)
N5−Cu−N2	91.20(7)	CuA−N2−Cu	101.92(7)
N1−Cu−N2	172.19(7)	N6−N5−Cu	126.36(15)

Table 3. Selected Bond Lengths (Å) and Angles (deg) for Compound **2**

Cu1−N2	1.940(2)	Cu2−N13	1.977(3)
Cu1−N4	1.943(3)	Cu2−N7	1.992(3)
Cu1−N3	2.035(3)	Cu2−N7B	2.040(3)
Cu1−N1	2.037(3)	Cu2−N4	2.374(3)
Cu1−N15A	2.358(3)	N7−Cu2B	2.040(3)
Cu2−N10	1.975(3)	N15−Cu1C	2.358(3)
N2−Cu1−N4	163.23(11)	N13−Cu2−N7B	88.65(11)
N2−Cu1−N3	80.00(11)	N7−Cu2−N7B	76.61(11)
N4−Cu1−N3	105.28(11)	N10−Cu2−N4	88.16(11)
N2−Cu1−N1	79.67(10)	N13−Cu2−N4	97.41(12)
N4−Cu1−N1	95.05(11)	N7−Cu2−N4	103.79(11)
N3−Cu1−N1	159.47(11)	N7b−Cu2−N4	91.02(10)
N2−Cu1−N15A	101.95(10)	N5−N4−Cu1	127.0(2)
N4−Cu1−N15A	94.19(11)	N5−N4−Cu2	115.3(2)
N3−Cu1−N15A	88.18(11)	Cu1−N4−Cu2	107.11(12)
N1−Cu1−N15A	93.20(10)	N8−N7−Cu2B	122.7(2)
N10−Cu2−N13	94.22(12)	Cu2−N7−Cu2B	103.39(11)
N10−Cu2−N7	100.87(11)	N11−N10−Cu2	123.9(2)
N13−Cu2−N7	154.23(13)	N14−N13−Cu2	124.2(2)
N10−Cu2−N7B	177.09(11)	N14−N15−Cu1C	114.5(2)

Table 4. Selected Bond Lengths (Å) and Angles (deg) for Compound **3**

Cu1−N4	1.950(4)	Cu2−N16	1.996(4)
Cu1−N2	1.951(4)	Cu2−N13	2.033(3)
Cu1−N3	2.032(3)	Cu3−N13	1.966(4)
Cu1−N1	2.034(3)	Cu3−N13A	1.966(4)
Cu1−N7	2.288(3)	Cu3−N16A	1.987(3)
Cu2−N10	1.941(4)	Cu3−N16	1.987(3)
Cu2−N7	1.956(3)		
N4−Cu1−N2	150.78(15)	N13−Cu3−N16A	100.78(15)
N4−Cu1−N3	95.54(14)	N13A−Cu3−N16A	79.22(15)
N2−Cu1−N3	79.45(14)	N13−Cu3−N16	79.22(15)
N4−Cu1−N1	103.01(14)	N13A−Cu3−N16	100.78(15)
N2−Cu1−N1	80.32(14)	N16A−Cu3−N16	180.000(1)
N3−Cu1−N1	159.69(15)	N5−N4−Cu1	131.9(3)
N4−Cu1−N7	105.46(15)	N8−N7−Cu2	120.4(3)
N2−Cu1−N7	103.43(14)	N8−N7−Cu1	114.4(3)
N3−Cu1−N7	91.27(13)	Cu2−N7−Cu1	117.84(16)
N1−Cu1−N7	91.69(13)	N11−N10−Cu2	126.4(3)
N10−Cu2−N7	97.93(16)	N14−N13−Cu3	126.8(3)
N10−Cu2−N16	167.54(15)	N14−N13−Cu2	125.1(3)
N7−Cu2−N16	93.83(15)	Cu3−N13−Cu2	101.14(16)
N10−Cu2−N13	90.18(15)	N17−N16−Cu3	130.1(3)
N7−Cu2−N13	164.50(15)	N17−N16−Cu2	127.6(3)
N16−Cu2−N13	77.43(14)	Cu3−N16−Cu2	101.68(16)
N13−Cu3−N13A	180.000(1)		

and distances for **1**−**3** are provided in the Supporting Information.

Compound **1** consists of stacks of neutral $[Cu_2(phprpy)_2$-μ-$(N_3)_2(N_3)_2]$ dimers (Figure 2a). Each centrosymmetric dimer consists of Cu^{2+} ions bridged by two end-on azido ligands. The Cu_2N_2 core is planar with a Cu−Cu distance of 3.100(1) Å and a Cu−N−Cu bridging angle is 101.92(7)°. The local coordination environment of each Cu^{2+} ion is an axially elongated octahedron with the equatorial plane defined by two nitrogen atoms from the intradimer end-on

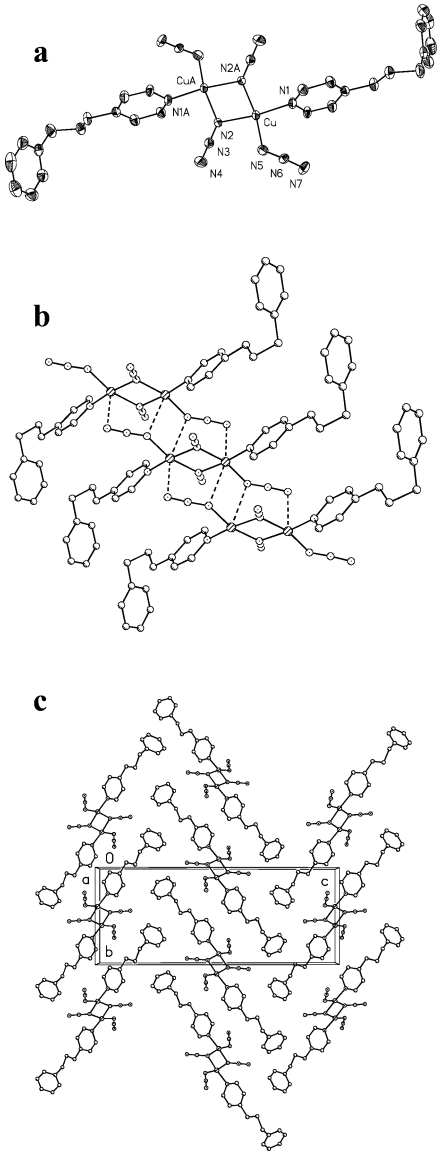

Figure 2. Crystal structure of $[Cu_2(phprpy)_2$-μ-$(N_3)_2(N_3)_2]$, **1**: (a) ORTEP plot (drawn to encompass 30% of electron density) of the formula unit with atomic numbering, (b) perspective view perpendicular to the stacking axis, and (c) packing diagram viewed parallel to the stacking axis. The disorderd portions of the organic ligands and hydrogen atoms have been removed for clarity.

azide bridges (N2 and N2A), one nitrogen atom from the monocoordinate azide ligand (N5), and one nitrogen atom from the pyridyl donor (N1) of phprpy. All equatorial Cu−N bond distances are in the range from 1.957(2) to 1.997(2) Å. In contrast, the axial positions are characterized by long Cu−N contacts of 2.620(2) and 3.140(2) Å to the monocoordinate azide ligands of adjacent dimers.

The dimers stack atop one another to form chains that extend along the crystallographic *a* axis (Figure 2b) and pack in a herringbone motif within the crystallographic *bc* plane (Figure 2c). The bridging azides are nearly linear (178.5°), whereas the terminal azide ligands are slightly bent (176.4°) at the central nitrogen atom. The coordinated phprpy ligands are disordered in the 1,3-propyl and pyridyl fragments. The phenyl groups of the organic ligands are not coplanar with the pyridyl moieties but twisted by 113.1° with respect to

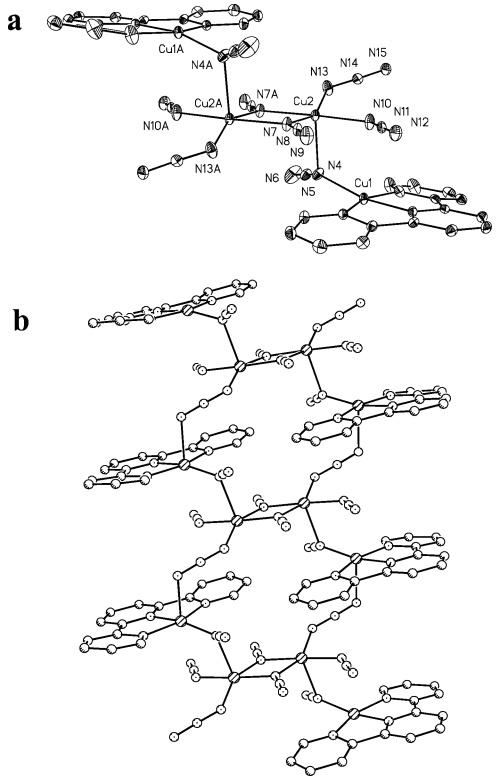

Figure 3. Crystal structure of $[Cu_2(terpy)_2$-μ-$(N_3)_4Cu_2$-μ-$(N_3)_2(N_3)_2]$, **2**: (a) ORTEP plot (drawn to encompass 30% of electron density) of the formula unit with atomic numbering, (b) perspective view perpendicular to the stacking axis. Hydrogen atoms have been removed for clarity.

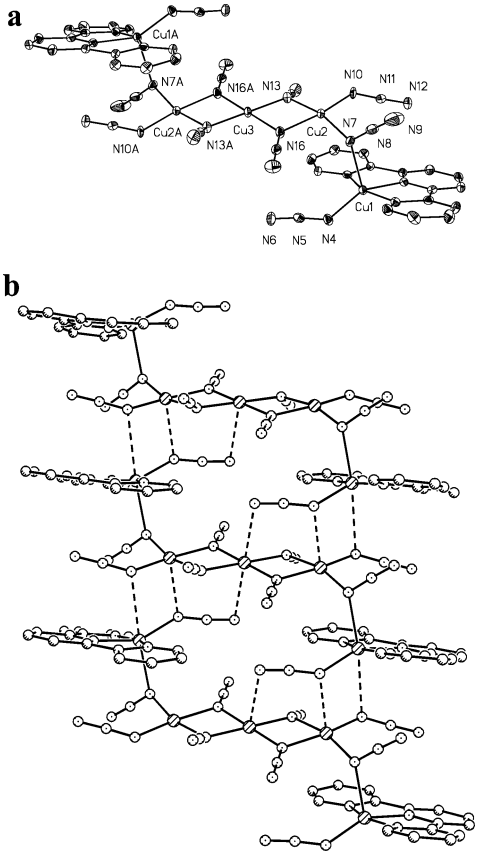

Figure 4. Crystal structure of $[Cu_2(terpy)_2$-μ-$(N_3)_2(N_3)_2Cu_3$-μ-$(N_3)_4(N_3)_2]$, **3**: (a) ORTEP plot (drawn to encompass 30% of electron density) of the formula unit with atomic numbering, (b) perspective view perpendicular to the stacking axis. Hydrogen atoms have been removed for clarity.

one another. The pyridyl group is twisted by 69.5(1)° out of the plane defined by the dinuclear Cu_2N_2 core. The structure of **1** bears close resemblance to that of $[Cu(4\text{-etpy})(N_3)_2]_2$ (4-etpy = 4-ethylpyridine), a ladder-like chain of weakly interacting end-on azido-bridged Cu(II) dimers.[41]

In compound **2**, dimeric $Cu_2(N_3)_4$ moieties are coordinated to chains of $Cu(terpy)(N_3)_2$ units to form neutral, ladder-like, azido-bridged coordination polymers that extend along the crystallographic *b* axis. The "rungs of the ladder" consist of centrosymmetric double end-on azide bridged Cu_2-μ-$(N_3)_2$-$(N_3)_2$ dimer units positioned parallel to the crystallographic *a* axis (Figure 3a). Along the "legs", these dimers are linked to monomeric $Cu(terpy)(N_3)_2$ units through alternating single end-to-end and end-on azide bridges (Figure 3b). The rung Cu^{2+} ions are five-coordinate, adopting a highly distorted square-pyramidal geometry. The basal plane is defined by a nitrogen atom from a monodentate azido ligand (N10), two nitrogen atoms from the doubly end-on bridging azido groups within the dimer (N7 and N7A), and one nitrogen atom from the single end-to-end azide (N13) bridge to an adjacent Cu(terpy) unit. The apical site is occupied by a nitrogen atom from a single end-on azide bridge to the other adjacent Cu(terpy) unit along the leg. The basal Cu−N bond distances range from 1.975(3) to 2.040(3) Å and are significantly shorter than the apical Cu−N bond of 2.374(3) Å. The trans N7−Cu2−N13 and N7A−Cu2−N10 angles in the basal plane are 154.2(1)° and 177.1(1)° and the N(basal)−Cu−N(apical) angles range from 88.2(1)° to 103.8(1)°, indicating significant deviation from ideal square-pyramidal geometry arising from the distortion of N13 out of the N7−N7A−N10−N13 mean plane. The cyclic Cu_2N_2 core is planar with a Cu2−Cu2A distance of 3.164(2) Å. Each Cu2−N−Cu2A bridge angle is 103.4(1)°, but the bridge is slightly asymmetric, with Cu2−N7 and Cu2−N7A bond distances of 1.992(3) and 2.040(3) Å, respectively.

The Cu^{2+} ions of the $Cu(terpy)(N_3)_2$ units of **2** adopt a slightly distorted square-pyramidal geometry. The basal plane is defined by three nitrogen atoms from the terpyridine ligand (N1, N2, and N3) and a nitrogen atom (N4) from the single end-on azide bridge to the rungs. The apical site (N15B) is occupied by the single end-to-end azido bridge to an adjacent rung dimer. The axial Cu1−N15B bond, 2.358(3) Å, is significantly longer than the basal Cu−N bond distances that range from 1.940(2) to 2.037(3) Å. This square pyramid is also distorted as the trans N1−Cu1−N3 and N2−Cu1−N4 basal plane angles are 163.2(1)° and 159.5(1)°, and the angles between the basal plane nitrogen atoms and the apical nitrogen atoms range from 88.2(1)° to 101.9(1)°.

Compound **3** contains neutral stacks of linear pentamer units, $Cu_5(terpy)_2(N_3)_{10}$. Each pentamer (Figure 4a) contains a center of inversion and consists of two terminal Cu(terpy)-$(N_3)_2$ moieties and a central Cu_3-μ-$(N_3)_4(N_3)_2$ fragment. The pentamer units stack along the crystallographic *a* axis (Figure 4b). The central Cu_3-μ-$(N_3)_4(N_3)_2$ fragment is itself composed

(41) Goher, M. A. S.; Escuer, A.; Mautner, F. A.; Al-Salem, N. A. *Polyhedron* **2001**, *20*, 2971.

of two types of metal centers. The Cu^{2+} ions at the ends of the trimer, Cu2 and Cu2A, are connected to the central ion, Cu3, through double end-on azide bridges thus forming two cyclic Cu_2N_2 units. The bridging azides are linear and the Cu_2N_2 units are planar. The Cu2−Cu3 distance is 3.089(1) Å, and the Cu2−N−Cu3 bridging angles are 101.7(2)°. The local geometry of the central copper ion is distorted octahedral. The equatorial plane is defined by four nitrogen atoms from the four azide bridges (N13, N16, N13A, and N16A), and the axial positions are formed by weak Cu3−N contacts [2.650(4) Å] to the terminal nitrogen atoms of the monocoordinate azide ligands on Cu(terpy)$(N_3)_2$ moieties from adjacent pentamers (Figure 4b). The copper ions at the ends of the trimer core adopt a distorted ssquare-pyramidal geometry. The basal plane is defined by two nitrogen atoms from the double end-on azide bridges (N13 and N16), a nitrogen atom from a monocoordinate azide ligand (N10), and a nitrogen atom (N7) from a single end-on azide bridge to the terminal Cu(terpy)$(N_3)_2$ groups. The apical site is occupied by the ligated nitrogen atom (N4) of the monodentate azide ligand of a Cu(terpy)$(N_3)_2$ moiety on an adjacent pentamer, and this contact [Cu2−N4 = 2.637(4) Å] is significantly longer than the basal bonds. In the basal plane, the Cu2−N bonds to the double end-on azide bridges are unequal [2.033(3) and 1.996(4) Å] but longer than the bonds to the single end-on azide bridge Cu2−N7 [1.956(3) Å] and the monodentate azide ligand Cu−N10 [1.941(4) Å]. The average value of the N(apical)−Cu−N(basal) bond angles is 93.4°, and the trans-basal N10−Cu−N16 and N13−Cu−N7 angles are 167.5(1)° and 164.5(1)°, respectively.

The Cu(terpy)$(N_3)_2$ units of **3** adopt a distorted square-pyramidal geometry. The basal plane is defined by three pyridyl nitrogen donors from the terpyridine ligand (N1, N2, and N3) and a nitrogen atom from a monocoordinate azide ion (N4). The apical site is occupied by a single end-on azide bridging ligand (N7) that links the terminal Cu^{2+} ions to the Cu_3-μ-$(N_3)_4(N_3)_2$ core. The bridge is asymmetric because the Cu1−N7 bond, 2.288(3) Å, is longer than the Cu2−N7 bond, 1.956(3) Å. The terminal square pyramids are axially elongated, as the Cu1−N7 bond is significantly longer than the basal Cu−N bonds [1.950(4)−2.032(3) Å]. The average value of the N(apical)−Cu1−N(basal) angles is 98.0°, and the trans-basal N1−Cu1−N3 and N2−Cu1−N4 angles are 159.7(1)° and 150.8(1)°, respectively.

Interesting structural features present in compounds **2** and **3** are the ladder-like topologies with varying types of azide bridges. Whereas compound **3** features both single and double end-on azide bridges, compound **2** contains both of these as well as single end-to-end bridges. Although single end-to-end bridges are known in Cu^{2+} complexes, single end-on azide bridges are still rare and generally occur only in the presence of other bridging groups.[11,12,29,42]

(42) Gao, E.-Q.; Bai, S.-Q.; Wang, C.-F.; Yue, Y.-F.; Yan, C.-H. *Inorg. Chem.* **2003**, *42*, 8456.

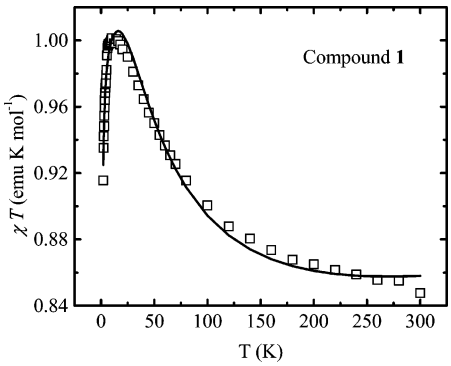

Figure 5. Magnetic properties measured for a powder sample of $[Cu_2(phprpy)_2$-μ-$(N_3)_2(N_3)_2]$, **1**. In the χT vs T plot (per Cu^{2+} dimer), the experimental data are given by the open boxes and the solid line refers to the best fit data, listed in Table 2, obtained using the spin dimer Hamiltonian, $\hat{H}_1$, from eq 1.

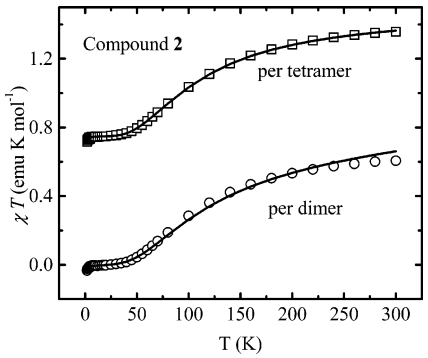

Figure 6. Magnetic properties measured for a powder sample of $[Cu_2(terpy)_2$-μ-$(N_3)_4Cu_2$-μ-$(N_3)_2(N_3)_2]$, **2**. The experimental data are given by the open boxes (per Cu^{2+} tetramer), and the solid line refers to the best fit, using parameters in Table 2 and the spin tetramer Hamiltonian, $\hat{H}_2$, from eq 2. The open circles are the data (per dimer) after subtraction of the contribution from the terminal Cu(terpy) sites assuming that they are noninteracting. The fit corresponds to the best fit to the spin dimer Hamiltonian, $\hat{H}'_2$, from eq 6, given by the parameters in Table 2.

Magnetic Properties. The χT vs T plot for **1** is shown in Figure 5 as open squares. The χT value at room temperature corresponds to 0.423 emu K mol^{-1} of Cu^{2+} ions, and as the temperature is lowered, χT increases, indicating dominant ferromagnetic interactions. Below 10 K, χT decreases and approaches zero, suggesting weaker intermolecular antiferromagnetic interactions. For compound **2**, the χT value decreases as temperature is lowered, indicating antiferromagnetic exchange, until reaching a plateau below 50 K (Figure 6). A consequence of the strong antiferromagnetic interactions is that the room-temperature value of χT (0.39 emu K mol^{-1} of Cu^{2+} ions) is lower than for compound **1**. Below 5 K, the χT value decreases further toward zero. The χT vs T plot for **3** is shown in Figure 7. As the temperature is lowered, χT increases because of dominant ferromagnetic interactions until reaching a maximum value at 6.5 K and then decreases toward zero.

Analysis of Magnetic Properties. Compounds **1**−**3** contain neutral stacks of dimers, linear tetramers, and linear pentamers, respectively. For each, magnetic interactions between these oligomeric units along the ladder legs are expected to be small, a consequence of long Cu−N distances. Thus, the magnetic states of the oligomers in **1**−**3** can be

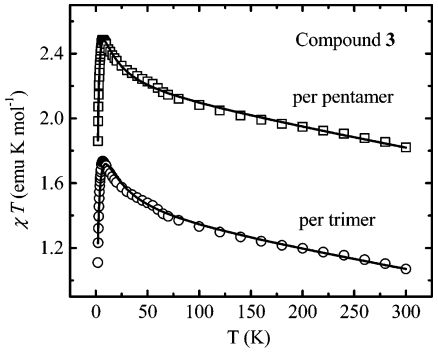

Figure 7. Magnetic properties measured for a powder sample of $[Cu_2(terpy)_2$-μ-$(N_3)_2(N_3)_2Cu_3$-μ-$(N_3)_4(N_3)_2]$, **3**. The experimental data are given by the open boxes (per Cu^{2+} pentamer) and the solid line refers to the best fit of the data (Table 2) obtained using the spin pentamer Hamiltonian, $\hat{H}_3$, from eq 3. The open circles are the data (per trimer) after subtracting the contribution from the terminal Cu(terpy) sites assuming that they are noninteracting. The corresponds to the best fit to the spin trimer Hamiltonian, $\hat{H}'_3$, from eq 7, with the parameters in Table 2.

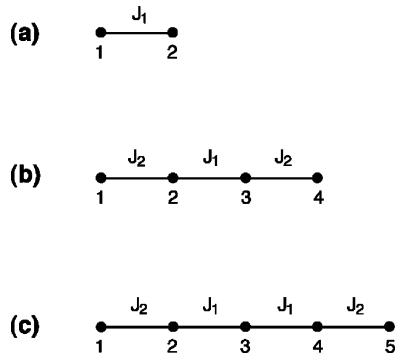

Figure 8. Parameters and spin-site connectivity defining (a) the spin dimer Hamiltonian $\hat{H}_1$, (b) the spin tetramer Hamiltonian $\hat{H}_2$, and (c) the spin pentamer Hamiltonian $\hat{H}_3$.

described as depicted in Figure 8 and by the Heisenberg spin Hamiltonians $\hat{H}_1$, $\hat{H}_2$, and $\hat{H}_3$, respectively

$$\hat{H}_1 = -2J_1(\hat{S}_1 \cdot \hat{S}_2) \tag{1}$$

$$\hat{H}_2 = -2J_1(\hat{S}_2 \cdot \hat{S}_3) - 2J_2(\hat{S}_1 \cdot \hat{S}_2 + \hat{S}_3 \cdot \hat{S}_4) \tag{2}$$

$$\hat{H}_3 = -2J_1(\hat{S}_2 \cdot \hat{S}_3 + \hat{S}_3 \cdot \hat{S}_4) - 2J_2(\hat{S}_1 \cdot \hat{S}_2 + \hat{S}_4 \cdot \hat{S}_5) \tag{3}$$

Once the spin Hamiltonian is specified for an isolated oligomer, its magnetic energy levels can be calculated as a function of the spin exchange parameters, allowing the van Vleck magnetic susceptibility, χ_{vv}, of the oligomer to be calculated as a function of temperature. Weak spin exchange interactions can take place between adjacent oligomers, so that a more appropriate quantity to consider is the Weiss susceptibility χ_w

$$\chi_w = \frac{\chi_{vv}}{1 - (zJ'/N_A g^2 \beta^2)\chi_{vv}} \tag{4}$$

where J' is the spin exchange parameter between adjacent oligomers, g is the g value, β is the Bohr magneton, and z is the number of nearest-neighbor oligomers surrounding one oligomer. The experimental magnetic susceptibility, χ_{exp}, already corrected for core diamagnetism, also includes the temperature-independent term, χ_0, which refers to the sum of the temperature-independent paramagnetism (>0) and the diamagnetism (<0). In addition, samples used for magnetic susceptibility measurements invariably contain a trace amount of magnetic impurities. The susceptibility arising from the impurities, χ_{imp}, is expected to follow the Curie law, $\chi_{imp} = C'/T$, where C' is a constant. Consequently, the experimental susceptibility χ_{exp} can be simulated with the calculated susceptibility χ_{cal}

$$\chi_{cal} = \chi_w + \chi_0 + \chi_{imp} = \frac{\chi_{vv}}{1 - (zJ'/N_A g^2 \beta^2)\chi_{vv}} + \chi_0 + \frac{C'}{T} \tag{5}$$

using J_1, J_2, and the zJ', g, C', and χ_0 terms as fitting parameters. The fitting results for compounds **1**−**3** are listed in Table 5 and superimposed on the data in Figures 5−7.

For compound **1**, the simulation is consistent with strong ferromagnetic intradimer coupling ($2J = 73.8$ K) and very weak antiferromagnetic exchange ($zJ' = -0.15$ K) between the dimers. The fitted g value ($g = 2.02$) is consistent[43] with an axially elongated octahedral Cu^{2+} and agrees with the room-temperature X-band measurement of $g = 2.0$. The fit slightly overestimates the maximum in χT, which could be due to additional exchange interactions or zero-field splitting of the triplet ground state. The field-dependent magnetization, M vs H, approaches 1.1×10^4 emu G mol^{-1} at saturation, corresponding to a total spin of $S = 1$ per dimer (Supporting Information). The experimental data approach saturation more quickly than predicted by an $S = {}^1/_2$ Brillouin function, but closely follow the $S = 1$ Brillouin function, further supporting the presence of strong, intradimer ferromagnetic coupling.

Ferromagnetic exchange in **1** is consistent with the small Cu−N−Cu bridging angle of 101.9°, as has been observed with similar μ-diazido-bridged dinuclear copper(II) complexes.[6,7,11,44,45] The large magnitude of the coupling constant is reasonable for the small bridging angle, the short Cu−(bridging)N bonds, the planar Cu_2N_2 core geometry, and the double end-on azido ligands that bridge equatorial−equatorial coordination sites. The weak antiferromagnetic coupling between dimers is consistent with the long Cu−N bond distances and the asymmetric end-on and end-to-end azide bridging between Cu(II) sites.

For compound **2,** the fit indicates very strong antiferromagnetic exchange ($2J_1 = -200$ K) within the core dimer. The exchange interaction J_2 becomes important below 50 K but is at least an order of magnitude smaller than J_1. Field-dependent magnetization of compound **2** (Supporting Information) supports the conclusions drawn from the susceptibility data. At 5 T, the highest field measured, the magnetization appears to approach saturation near 1.1×10^4 emu G mol^{-1}, corresponding to a total spin of $S = 1$ per

(43) Abragam, A.; Bleaney, B. *Electron Paramagnetic Resonance of Transition Ions*; Oxford University Press: London, 1970.
(44) Manikandan, P.; Muthukumaran, R.; Thomas, K. R. J.; Varghese, B.; Chandramouli, G. V. R.; Manoharan, P. T. *Inorg. Chem.* **2001**, *40*, 2378.
(45) Albada, G. A. V.; Lakin, M. T.; Veldman, N.; Spek, A. L.; Reedijk, J. *Inorg. Chem.* **1995**, *34*, 4910.

Table 5. Values of the Parameters g, $2J$, $2J'$, zJ', χ_0, χ_D, and C' Determined for **1**−**3** from Fitting Analysis of Their Magnetic Susceptibilities[a]

compd/Hamiltonian used		g	$2J_1$	$2J_2$	zJ'	χ_0	C'	sd[b]
1	dimer	2.02	73.8		−0.15	1.66×10^{-4}	1.73×10^{-3}	2.6×10^{-5}
2	tetramer	2.00	−200	−11.8	0.02	8.54×10^{-5}	1.89×10^{-4}	1.9×10^{-5}
	dimer	1.92	−219		−0.75	-4.20×10^{-4}	9.63×10^{-3}	8.8×10^{-2}
3	pentamer	2.15	15.9	−2.97	0.00	-1.21×10^{-3}	2.57×10^{-4}	2.1×10^{-5}
	trimer	2.17	21.6		−0.70	-1.13×10^{-3}	5.34×10^{-2}	5.6×10^{-4}

[a] $2J_1$, $2J_2$, and zJ' are in units of K, χ_0 is in units of emu/mol, and C' is in units of emu K/mol. [b] Standard deviation of the fit.

tetramer. This observation is consistent with the presence of a strong intradimer exchange term, J_1, so that, at 2 K, only the weaker interactions, J_2 and zJ',are perturbed by the 5-T applied field. The strongly antiferromagnetically coupled dimer core should not saturate at experimentally accessible magnetic fields. Also, it should be noted that this strongly antiferromagnetic J_1 causes the $\chi_M T$ vs T response to be independent of the sign of J_2, as both ferromagnetic and antiferromagnetic J_2 terms give rise to a nonmagnetic ground state for the tetramer.

For compound **3**, weak ferromagnetic exchange ($2J_1 =$ 15.9 K) is indicated within the trimeric core, with much weaker antiferromagnetic interactions between the trimer and the terminal Cu(terpy) units. The fitted g values ($g = 2.15-2.17$) are consistent with square-pyramidal Cu^{2+} ions[43] and agree with the value of $g = 2.14$ measured at room temperature by X-band ESR spectroscopy. The field dependent magnetization data (Supporting Information) approaches 2.5×10^4 emu G mol^{-1} at saturation, corresponding to a total spin of $S = {}^5/_2$ per pentamer.

The spin exchange interactions within the cores of oligomers **2** and **3** present puzzling features. The most surprising observation is the strong antiferromagnetic exchange, J_1, between the central Cu^{2+} ions of **2**. The short Cu−N bonds, the planarity of the cyclic Cu_2N_2 moiety, and the double end-on azido ligands that bridge basal−basal coordination sites are expected to make J_1 the strongest interaction within the tetramer, but the sign of J_1 is not consistent with those of other similar di-μ-azido-bridged copper(II) complexes. Calculations and magnetostructural correlations predict that, for double end-on azido-bridged Cu^{2+} units, the angle of accidental orthogonality is approximately 103° and ferromagnetic exchange is expected for bridging angles close to this value.[1,11,12,16] For example, the bridging angle in **2** (103.4°) is essentially the same as in the di-μ-azido copper dimer $Cu_2(N_3)_4(C_{16}H_{34}N_2O_6)$ (103.6°) studied by Kahn,[9] for which a moderately strong ferromagnetic coupling was observed. Also, for **3**, although the positive sign of the intratrimer coupling constant, J_1, is consistent with the small Cu−N−Cu angle of 101.7° formed by the double end-on azido bridges, the magnitude of the ferromagnetic coupling constant is much smaller than that observed for similar μ-diazido-bridged copper(II) complexes.

Qualitative orbital interaction arguments suggest that the different exchange interactions in **2** and **3** result from the coordination geometry of the copper ions. The magnetic orbital of a Cu^{2+} ion in an axially elongated octahedral or a square-pyramidal site is given by the Cu 3d x^2-y^2 orbital contained in the basal plane, which forms σ antibonding interactions with the orbitals of the four surrounding basal ligand atoms. Strong exchange interactions, either ferromagnetic or antiferromagnetic, between adjacent Cu^{2+} sites can occur only when their magnetic orbitals are contained in a same plane.[1,9,46] In **2**, the basal planes of copper ions in the dimeric core are highly distorted. The average value of the N(apical)−Cu−N(basal) bond angles is 95.1°, and the trans-basal N10−Cu−N16 and N13−Cu−N7 angles are 154.2(1)° and 177.1(1)°, respectively. The extent of distortion from square-pyramidal geometry can be quantified with the parameter $\tau = |\beta - \alpha|/60$, where β and α are the bond angles of the trans donor atoms in the basal plane.[47] For ideal square-pyramidal coordination, $\tau = 0$, whereas for a trigonal bipyramid, $\tau = 1$. The distortion parameter for Cu2 in compound **2** is 0.38, indicating a highly distorted square-pyramidal environment with significant trigonal bipyramidal character. This distortion removes the orthogonality that exists between the magnetic orbitals if the Cu^{2+} ions in the Cu_2N_2 core are both planar and leads to significant overlap between these magnetic orbitals, giving rise to the strong antiferromagnetic exchange. In contrast, the copper ions at the ends of the trimer core of **3** adopt an only slightly distorted ssquare-pyramidal geometry, with $\tau = 0.05$ for Cu2. The slight distortion reduces the ferromagnetic component, but this component still dominates the total exchange.

Simplified Model. In this section, we attempt to quantitatively correlate the spin exchange interactions in **1**−**3** with their electronic structure using Spin Dimer Analysis. To do so, it is easier to focus on the predominant exchange interactions and ignore the secondary interactions. For example, the strongly interacting spin units of **1** are isolated dimers, $Cu_2(N_3)_6(phprpy)_2$ (Figure 9a), and intermolecular interactions are much weaker than the intradimer exchange. For compound **2**, electronic interactions between Cu1 and Cu2 are weak, a consequence of the equatorial to axial bridges. Therefore, as in compound **1**, the strongly interacting spin units of **2** are dimers, the central $Cu_2(N_3)_8$ units (Figure 9b). In compound **3**, the Cu1−Cu2 linkage is also an axial-to-equatorial bridge, leaving the central $Cu_3(N_3)_{10}$ trimers as the only strongly interacting spin units (Figure 9c).

To support the validity of these considerations, the temperature-dependent magnetization data were simulated using simplified Hamiltonians. Thus, the spin Hamiltonian $\hat{H}_2$ for **2** can be simplified as

$$\hat{H}_2' = -2J_1(\hat{S}_2 \cdot \hat{S}_3) \qquad (6)$$

(46) Tuczek, F.; Bensch, W. *Inorg. Chem.* **1995**, *34*, 1482.
(47) Addison, A. W.; Rao, T. N. *J. Chem. Soc., Dalton Trans.* **1984**, 1349.

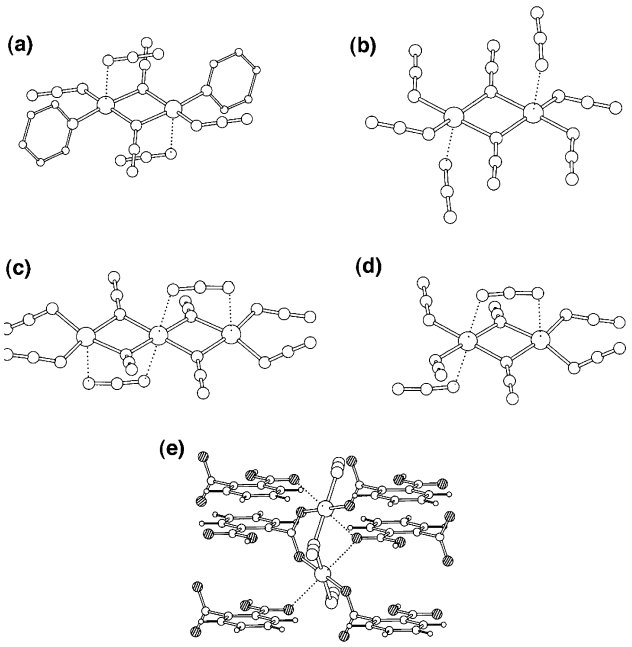

Figure 9. Strongly interacting spin units in compounds **1**−**3** and Cu(Hpht)$(N_3)(H_2O)$. (a) Spin dimer $Cu_2(N_3)_6(phprpy)_2$ in **1**, where the phprpy ligands are represented by showing only the pyridyl moieties. (b) Spin dimer $Cu_2(N_3)_8$ dimer in **2**. (c) Spin trimer $Cu_3(N_3)_{10}$ in **3**. (d) Spin dimer $Cu_2(N_3)_8$ in **3**, which is a part of the spin trimer. (e) Spin dimer $Cu_2(N_3)_3(Hpht)_6$ in Cu(Hpht)$(N_3)(H_2O)$.

by assuming that spin sites 1 and 4 (Figure 8) do not interact with the central spin dimer. Likewise, the spin Hamiltonian $\hat{H}_3$ for **3** can be simplified as

$$\hat{H}'_3 = -2J_1(\hat{S}_2 \cdot \hat{S}_3 + \hat{S}_3 \cdot \hat{S}_4) \qquad (7)$$

under the assumption that spin sites 1 and 5 (Figure 8) do not interact with the central spin trimer. It should be noted that the χ_{exp} values of **1**−**3** are normalized to their formula units, so to fit the χ_{exp} data of **2** and **3** in terms of the Hamiltonians $\hat{H}'_2$ and $\hat{H}'_3$, respectively, it is necessary to subtract from the χ_{exp} data the Curie paramagnetic susceptibility associated with the two noninteracting Cu^{2+} ions, the Cu(terpy)$(N_3)_2$ moieties that are ignored in eqs 6 and 7. The simulations using these simplified models for **2** and **3** are included in Figures 6 and 7, and the values of the fitting parameters are listed in Table 5. These simplified models reproduce the data reasonably well and yield values for the principal exchange constants, J_1, that are similar to those obtained using the more complete Hamiltonians, $\hat{H}_2$ and $\hat{H}_3$. On the other hand, in compound **2**, the dimer model can be too simplified as it ignores the appreciable interdimer exchange J_2, which is too large in magnitude to be treated as a molecular field correction and significantly underestimates the g value.

Spin Dimer Analysis. In terms of first-principles electronic structure calculations, the signs and strengths of spin exchange interactions (i.e., spin exchange parameters, J) are calculated for the high- and low-spin states of spin dimers (i.e., structural units consisting of two spin sites)[48−50] and

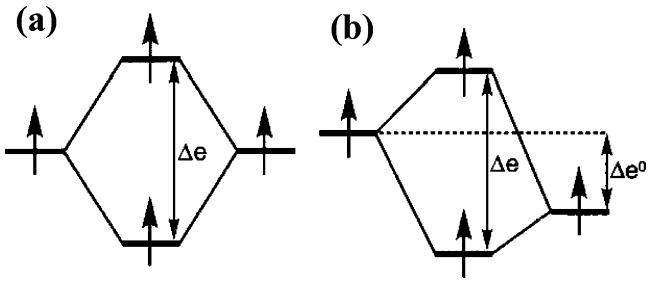

Figure 10. Interaction between adjacent magnetic orbitals leading to the spin−orbital interaction energy: (a) between equivalent spin sites and (b) between nonequivalent spin sites.

by electronic band structure calculations for various ordered spin arrangements of a magnetic solid.[51] For magnetic solids with large and complex unit cell structures, these quantitative methods become difficult to apply. To understand physical properties of magnetic solids, however, it is often sufficient to estimate the relative magnitudes of the J values.[1,8,36] In general, a spin exchange parameter J between two adjacent spin sites consists of two components, $J = J_F + J_{AF}$. The ferromagnetic term J_F (> 0) is proportional to the exchange integral K_{12} between the magnetic orbitals ϕ_1 and ϕ_2 representing the two spin sites. The component J_F is small so that the spin exchange becomes ferromagnetic (i.e., $J > 0$) only when the antiferromagnetic term J_{AF} (<0) is negligibly small in magnitude. For a spin dimer with two equivalent spin sites, J_{AF} varies as $J_{AF} \propto -(\Delta e)^2$,[1] where Δe is the spin−orbital interaction energy (Figure 10a) between the two magnetic orbitals ϕ_1 and ϕ_2. If the two spin sites are not equivalent such that their magnetic orbitals differ in their energy levels by Δe^0, then J_{AF} is proportional to $-(\Delta\epsilon)^2$, where $\Delta\epsilon = \sqrt{(\Delta e)^2 - (\Delta e^0)^2}$ (Figure 10b).[1] For a spin dimer of two equivalent spin sites, $\Delta e^0 = 0$, so that $(\Delta\epsilon)^2 = (\Delta e)^2$, and hence, the notation $(\Delta\epsilon)^2$ will be used to refer to the case of spin dimers with equivalent spin sites as well. To probe the puzzling aspects of the spin exchange parameters mentioned in the previous section, we determine the $(\Delta\epsilon)^2$ values for the strongest spin exchange paths in compounds **1**−**3** using extended Hückel tight-binding (EHTB) calculations[52,53] for the spin dimers representing these paths. These spin dimers are $Cu_2(N_3)_6(phprpy)_2$ (Figure 9a) for **1** and $Cu_2(N_3)_8$ (Figure 9b and d) for **2** and **3**. For our calculations, the dimer $Cu_2(N_3)_6(phprpy)_2$ was simplified by $Cu_2(N_3)_6(pyridine)_2$ upon replacement of the phprpy ligands with pyridines.

The $(\Delta\epsilon)^2$ values determined from EHTB calculations are quite sensitive to the types of Slater-type orbitals (STOs) used for atomic orbitals.[36] The parameters of the atomic orbitals used for extended Hückel tight-binding calculations are summarized in Table S13 in the Supporting Information. In our study, the Cu 3d orbitals were represented by double-ζ (DZ) STOs,[54] and the Cu 4s/4p orbitals by single-ζ (SZ)

(48) Illas, F.; Moreira, I. d. P. R.; Graaf, C. D.; Barone, V. *Theor. Chem. Acc.* **2000**, *104*, 265.
(49) Noodleman, L. *J. Chem. Phys.* **1981**, *74*, 5737.
(50) Dai, D.; Whangbo, M.-H. *J. Chem. Phys.* **2003**, *118*, 29.
(51) Derenzo, S. E.; Klitenberg, M. K.; Weber, M. J. *J. Chem. Phys.* **2000**, *112*, 2074.
(52) Hoffmann, R. *J. Chem. Phys.* **1963**, *39*, 1397.
(53) Dai, D.; Ren, J.; Liang, W.; Whangbo, M.-H.
(54) Clementi, E.; Roetti, C. **1974**, *14*, 177.

Table 6. Values of $(\Delta\epsilon)^2$ Calculated for the Spin Dimers Representing the Strongest Spin Exchange Paths in **1**−**3** and Cu(Hpht)(N_3)(H_2O)[a]

compd	spin dimer	atomic orbitals DZ/SZ[b]	atomic orbitals DZ/DZ[b]	atomic orbitals DZ/(DZ,SZ)[b]	J_{expt} (K)
1	$Cu_2(N_3)_6(phprpy)_2$	223 000	13 000	4000	73.8[c]
2	$Cu_2(N_3)_8$	75 400	11 800	11800	−200[c]
3	$Cu_2(N_3)_8$	184 000	900	900	15.9[c]
Cu(Hpht)(N_3)(H_2O)	$Cu_2(N_3)_3(Hpht)_6$	19 100	85 700	1800	108[d]

[a] $(\Delta\epsilon)^2$ is in units of $(meV)^2$. [b] See the text for the definitions. [c] This work [d] Reference 55.

STOs. However, the ligand atoms were represented by either DZ or SZ STOs as described below. In one set of calculations (referred to as the DZ/SZ calculations), SZ STOs were used for all ligand atoms. In the second set of calculations (referred to as the DZ/DZ calculations), DZ STOs were used for all ligand atoms. In the third set of calculations [referred to as the DZ/(DZ,SZ) calculations], the nitrogen atoms of the azide ions were represented by DZ STOs, but all other ligand atoms by SZ STOs. Results of our calculations are summarized in Table 6.

To explain the observed trends in the spin exchange interactions of compounds **1**−**3**, the $(\Delta\epsilon)^2$ values should be small for the spin dimers of **1** and **3**, which show ferromagnetic coupling, but large for the spin dimer of **2**, which shows antiferromagnetic coupling. This expectation is reproduced only by the DZ/(DZ,SZ) calculations, in which the azide ions are represented by the DZ STOs and the pyridyl ligands by the SZ STOs. This is understandable because the nitrogen atom orbitals of the azide anion should be more diffuse than those of the neutral pyridyl ligands. To test the generality of this observation concerning the effect of mixed ligands on $(\Delta\epsilon)^2$, we examine the spin exchange interaction in Cu(Hpht)(N_3)(H_2O) (Hpht = hydrogen phthalate),[55] in which adjacent Cu^{2+} ions are ferromagnetically coupled although the Cu−N−Cu angle associated with the end-on azide bridging is large (i.e., 111.9°). The spin dimer of this compound, $Cu_2(N_3)_3(Hpht)_6$ shown in Figure 9e, has two different ligands, i.e., the N_3^- and $Hpht^-$ anions. The basal plane of each Cu^{2+} site is coordinated by the N_3^- anion and the carboxylate group of the $Hpth^-$ anion. Results of our DZ/SZ, DZ/DZ and DZ/(DZ,SZ) calculations for the spin dimer $Cu_2(N_3)_3(Hpht)_6$ of Cu(Hpht)(N_3)(H_2O) are included in Table 6. As in the case of the spin dimer of **1**, the $(\Delta\epsilon)^2$ value of the spin dimer $Cu_2(N_3)_3(Hpht)_6$ becomes small with the DZ/(DZ,SZ) calculations, i.e., when the azide ion is represented by the DZ STOs and the Hpht ligand by SZ STOs. This is understandable because the nitrogen atom orbitals of the azide anion should be more diffuse than those of the carboxylate oxygen atom orbitals of the $Hpht^-$ anion.

The first result is that, for both **2** and **3**, the $\langle\Delta\epsilon^2\rangle$ values for the exchange pathway between the Cu1 and Cu2 sites are calculated to be zero, indicating that the central $Cu_2(N_3)_4$ dimers and $Cu_3(N_3)_6$ trimers do not interact with the peripheral Cu(terpy)(N_3)$_2$ moieties, a consequence of the apical-to-basal azide bridging. Thus, compounds **2** and **3** consist essentially of noninteracting stacks of dimers and trimers, respectively. In compound **2**, the calculated $\langle\Delta\epsilon^2\rangle$ value is large within the core dimer such that J_{AF} dominates the total exchange, $J = J_F + J_{AF}$, thus giving rise to the strong antiferromagnetic coupling, consistent with the analysis of the magnetic susceptibility data. In contrast, in **3**, both $\langle\Delta\epsilon^2\rangle$ and J_{AF} are small such that J_F dominates the total exchange. Even though the spin dimers of **2** and **3** are similar in that they both consist of only the azide ligands and the Cu^{2+} ions, the $\langle\Delta\epsilon^2\rangle$ value is much smaller for the spin dimer of **3** than for that of **2** because the spin dimer of **3** has nonequivalent Cu^{2+} ions but that of **2** has equivalent Cu^{2+} ions.

Conclusions

In the present work, we prepared three azido-bridged Cu^{2+} ladder-like coordination polymers, $[Cu_2(phprpy)_2$-μ-$(N_3)_2$-$(N_3)_2]$, **1**; $[Cu_2(terpy)_2$-μ-$(N_3)_4Cu_2$-μ-$(N_3)_2(N_3)_2]$, **2**; and $[Cu_2(terpy)_2$-μ-$(N_3)_2(N_3)_2Cu_3$-μ-$(N_3)_4(N_3)_2]$, **3**, and characterized their crystal structures and magnetic properties. Although the Cu^{2+} ions of these compounds have ladder-like arrangements, the magnetic structures of these compounds are best described as isolated dimers for **1** and **2** and as isolated trimers for **3**, because of the anisotropic shape and nodal properties of the Cu^{2+} magnetic orbitals. The spin dimers mediating strong spin exchange paths in **1**−**3** have in common double end-on azide bridges linking adjacent Cu^{2+} ions. Although these spin dimers exhibit similar bridging structures, the spin dimer of **1** exhibits a strong ferromagnetic coupling; that of **2**, a strong antiferromagnetic coupling; and that of **3**, a weak ferromagnetic coupling. These observations are apparently puzzling from the viewpoint of the usual structure−property correlation, which is based on the geometry and electronic structure considerations of the metal−ligand−metal superexchange paths. The observed trends in the spin exchange interactions of **1**−**3** are well explained using the spin dimer analysis based on the DZ/(DZ,SZ) calculations. Our study shows that the nature and geometry of the nonbridging ligands can have a strong influence on whether the spin exchange interaction between Cu^{2+} ions connected by double end-on azide bridging is ferromagnetic or antiferromagnetic.

Acknowledgment. Partial support from the Petroleum Research Fund, administered by the American Chemical Society, 36163-AC5, is gratefully acknowledged (M.W.M. and D.R.T.). This work was also partially supported by the National Science Foundation through Grants DMR-9900855 (D.R.T.) and DMR-0305371 (M.W.M.). K.A.A. acknowledges the National Science Foundation and the University of Florida for funding of the purchase of the X-ray equip--

(55) Escuer, A.; Vicente, R.; Mautner, F. A.; Goher, M. A. S. *Inorg. Chem.* **1997**, *36*, 1233.

ment. Work at North Carolina State University was supported by the Office of Basic Energy Sciences, Division of Materials Sciences, U.S. Department of Energy, under Grant DE-FG02-86ER45259. We gratefully acknowledge the contributions of D. Stratakis during the acquisition of the magnetic data and of B. C. Watson during the early stages of the data analysis.

Supporting Information Available: Tables of atomic coordinates and thermal displacement parameters and complete listings of bond angles and distances for **1**−**3**, magnetization vs applied field data for **1**−**3**, and parameters used for extended Hückel tight-binding calculations. This material is available free of charge via the Internet at http://pubs.acs.org.

IC049175Q